Massively parallel classical logic via coherent dynamics of an ensemble of quantum systems with dispersion in size

Hugo Gattuso[a], R. D. Levine[b,c,d,1], and F. Remacle[a,b]

[a]Theoretical Physical Chemistry, Unité de Recherche Molecular Systems B6c, University of Liège, B4000 Liège, Belgium; [b]The Fritz Haber Center for Molecular Dynamics and Institute of Chemistry, The Hebrew University of Jerusalem, Jerusalem 91904, Israel; [c]Department of Chemistry and Biochemistry, David Geffen School of Medicine, University of California, Los Angeles, CA 90095; and [d]Department of Molecular and Medical Pharmacology, David Geffen School of Medicine, University of California, Los Angeles, CA 90095

Contributed by R. D. Levine, June 24, 2020 (sent for review April 30, 2020; reviewed by Yoram Alhassid and Sabre Kais)

Quantum parallelism can be implemented on a classical ensemble of discrete level quantum systems. The nanosystems are not quite identical, and the ensemble represents their individual variability. An underlying Lie algebraic theory is developed using the closure of the algebra to demonstrate the parallel information processing at the level of the ensemble. The ensemble is addressed by a sequence of laser pulses. In the Heisenberg picture of quantum dynamics the coherence between the N levels of a given quantum system can be handled as an observable. Thereby there are N^2 logic variables per N level system. This is how massive parallelism is achieved in that there are N^2 potential outputs for a quantum system of N levels. The use of an ensemble allows simultaneous reading of such outputs. Due to size dispersion the expectation values of the observables can differ somewhat from system to system. We show that for a moderate variability of the systems one can average the N^2 expectation values over the ensemble while retaining closure and parallelism. This allows directly propagating in time the ensemble averaged values of the observables. Results of simulations of electronic excitonic dynamics in an ensemble of quantum dot (QD) dimers are presented. The QD size and interdot distance in the dimer are used to parametrize the Hamiltonian. The dimer N levels include local and charge transfer excitons within each dimer. The well-studied physics of semiconducting QDs suggests that the dimer coherences can be probed at room temperature.

noise resilience | 2D electronic spectroscopy | information quantal processing at room temperature | quantum dots | Lie algebra

Experimental quantum computing based on coupled two-level systems (qubits) is making impressive progress (1, 2), and equally important, algorithms that take advantage of the new capabilities for linear algebra operations essential to machine learning and artificial intelligence are being actively developed (3–6). Such algorithms include principal component analysis, which is used extensively to compact data. In chemical physics, NMR spectroscopy has received particular attention, initially driven by the analogy that a spin 1/2 nucleus is a two-level system. This is aided by the exquisite control that is possible over radio frequency pulses. Developments of algorithms for applications in the chemical sciences is also very active (7). Information theoretic related techniques offered by chemical physics include chemical kinetics and spectroscopy (8). Our work below takes particular advantage of progress in two-dimensional electronic spectroscopy (2DES) (9–11). Certain aspects of how we use the 2D coherence maps to perform logic have already been reported (12–14). Another area of chemical physics and material science that informs our work is the spectroscopy of semiconducting quantum dots (QDs) (15–24). Colloidal QDs have an inevitable size dispersion (25, 26). This dispersion is a source of noise in the coherence between states of QDs established by optical addressing, when averaged over the array. It is interesting to note that this noise turns out to be similar to the effects of perturbations by the solvent in 2D spectroscopy (9–11, 27–34).

In this paper we discuss the information processing that can be achieved using the quantum dynamics of an N-level system as addressed by short laser pulses. The concrete realistic example is an array of semiconducting QD dimers where each dimer has $N = 8$ excited levels and even more when fine structure splittings are included. Using an algebraic approach we argue that such a device can perform a classical-like parallel logic on N^2 real-valued observables. The proposal is to address and read such an array. The optical addressing and reading are necessarily an average over many dimers. Because the array is a classical, incoherent, mixture of many quantum systems, the averages over the array can be read reliably even for noncommuting observables. To validate the proposed scheme we need to demonstrate why a single N-level system can perform parallel logic with an input provided by one or more laser pulses and with optical emission as the readout. The 2DES is the method that we highlight to implement this scheme (24). The inevitable size dispersion of semiconducting colloidal QDs means that the dot sizes are not identical, and it is necessary to average the response of the dots over the distribution of their size. We discuss two aspects of this averaging. The first is can we read the output reliably despite the size disorder. To answer this question we

Significance

There is a worldwide effort toward quantum technology. Information processing, sensing, communication, and related areas are getting much of the attention. The advantages offered by the quantum domain are well recognized and acclaimed. Proposed implementations rely on systems operating at rather low temperatures and on the need to isolate the system from outside sources of noise. We discuss a theoretical scheme that suggests operating with a classical collection of quantum systems. An experimental demonstration of the principle is available. The ensemble is an array of size-disordered quantum dots addressed and probed by laser pulses. The algebraic approach encodes information in the coherences between quantum levels of the dots and demonstrates resilience to size disorder.

Author contributions: R.D.L. and F.R. designed research; H.G., R.D.L., and F.R. performed research; H.G. and R.D.L. contributed new reagents/analytic tools; H.G., R.D.L., and F.R. analyzed data; and R.D.L. and F.R. wrote the paper.

Reviewers: Y.A., Yale University; and S.K., Purdue University West Lafayette.

The authors declare no competing interest.

[1]To whom correspondence may be addressed. Email: raphy@mail.huji.ac.il.

This article contains supporting information online at https://www.pnas.org/lookup/suppl/doi:10.1073/pnas.2008170117/-/DCSupplemental.

First published August 17, 2020.

compute the quantum dynamical response of each dot and then average the output over the size distribution. To generate a stable average we need to include thousands or more of dots. This gives rise to a practical question, can we perform the averaging over the distribution of sizes before computing the dynamics? If so, we only need to compute the quantum dynamics once. We show that as long as the size distribution does not qualitatively alter the energy spectrum of the dots, the averaging can be done first, resulting in an output that is approximate but quite accurate. Whether we average first or do the dynamics first and then average, the output shows dephasing in time of the $N(N-1)$ coherences between the N energy levels. The extent of dephasing depends on the breadth of size disorder, and we find that at the current capabilities of about 5% variation in the dot diameters, almost all $N(N-1)$ coherences are readable.

When we sample over enough dots the distribution of energy levels of dots of different size stabilizes, and as is to be expected from the general theory (35, 36), the distribution is well described by a Gaussian for widths of size distribution smaller than or equal to 5%. This enables us to compute the dephasing time scale analytically. One can expect on physical grounds that the coherence that is dephasing faster is between the higher electronically excited states of the dimers as these have the widest size-induced fluctuations in their energies. This, however, needs to be qualified because the oscillation period of the coherences is determined by the energy differences of the two levels. The energies of different levels can be correlated which will also affect the distribution of their difference.

Our model system is an ensemble of small (2 to 4 nm diameter) heterodimers of CdSe QDs as studied experimentally in ref. 37. The sizes of the two QDs in the dimer are selected so as to bring excitons into resonance, leading to efficient interdot coupling within the dimer. Individual CdSe QDs have received considerable theoretical attention (25, 38–44). Here we focus on dimers which exhibit a richer level structure, and we compute the dynamics for a very large number of dimers with slightly different dot sizes. We chose to use a model Hamiltonian based on the effective mass model with the **k.p** method (38, 40, 41, 45, 46) to describe an individual dot and describe the coupling with an excitonic Hamiltonian including both local and charge transfer (CT) excitons. As discussed before (47), this enables us to realistically model the effect of size variation of the individual dots and also account for variations in the interdot distance. We report first on the model electronic structure of the dimers in the ensemble with special reference to the distribution of energy levels and of the spacings between them. *SI Appendix*, section S1, provides more details. We induce transitions by a fast (and therefore broad in frequency) laser pulse. After this optical addressing is over, the coherences between two levels oscillate with the frequency that equals the spacing between the energies of these two levels. The size-induced dispersion in these spacings is what determines the dephasing time. *SI Appendix*, section S2, provides additional details about these distributions. Next we provide a brief outline of the dynamics of a single dimer under a laser addressing and of the kind of information processing that can be achieved when the dots are uniform in size. Using the results for computing the dynamics in the ensemble of dots of varying size, we discuss next that even in the case of small but realistic size dispersion one can still perform information processing. We outline how to first average over the size distribution and only then perform the dynamics, with more details given in *SI Appendix*, section S3. Last, we present our results (see also *SI Appendix*, section S4) and conclusions with the take-home message that information processing based on both the population of levels and their coherences is possible for a narrow but realistically finite size dispersion. This is because the output is optical and so can be read in a time shorter compared to the dephasing. It remains the case that any reduction in size dispersion will be very beneficial in considerably increasing the dephasing time.

The conclusion that size dispersion is tolerable but the lower the better raises the question of why not to use molecules (or, for that matter, stoichiometric dots). Such systems have no inherent fluctuations but are more susceptible to perturbations by the environment. The formalism for first averaging over the size distribution (see also *SI Appendix*, section S3) is also useful for such perturbations. The real issue is practical. We need logic units with a dense set of excited electronic states in the visible range of the spectrum where short femtosecond laser pulses are available so that many states of each unit are within the coherent bandwidth of the laser.

The Electronic States of the Dots and of the Dimer

Our purpose is to model the level structure of the individual dimers as a function of the size of the two monomeric QDs and of the QD separation. The energy resolution accuracy needs to be sufficient for the very fast dynamics, say below 250 fs, induced by a sequence of femtosecond laser pulses that is of interest in the 2D electronic spectroscopy that we use to address and read the ensemble (24). We model the isolated small CdSe QDs with radius smaller than the bulk Bohr radius of the excitons. The states are lowest eigenstates of a confining spherical well of finite depth. Solving the radial Schrödinger equation gives the hole and electron energies and wave functions as a function of the QD size.

Colloidal semiconducting QDs are synthesized with a finite size dispersion at best 5% in diameter (Fig. 1*A*). The energies of the hole and electron states depend on the dot size, and the dispersion in their energies with size gives rise to a dispersion in the spectral response. From these single-particle states, analogous to molecular orbitals, one forms all possible many-electron

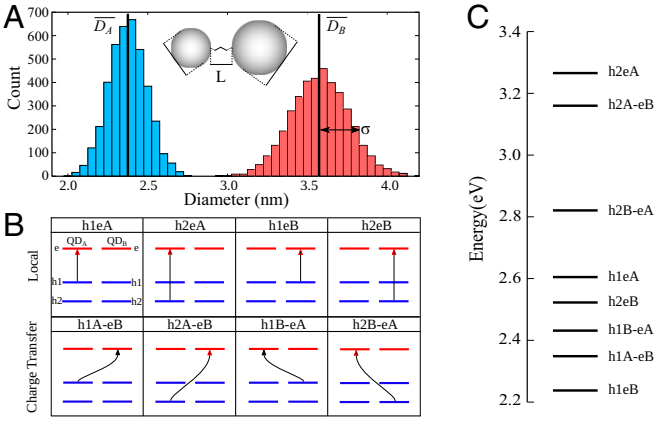

Fig. 1. Building the electronic states of the ensemble. (*A*) The Gaussian size distribution of the two dots, QDA and QDB, that make a dimer. Each distribution is characterized by a mean value of the diameter, $\overline{D}_A$ and $\overline{D}_B$, and an SD σ_A and σ_B, respectively. (*B*) Excitations leading to the zero-order exciton states built upon two hole states (h1 and h2; blue bars) and one electron (e; red bars) state per dot. Eight exciton states can be constructed, four local excitons, i.e., h1eA (*Top*), where the hole–electron pair is localized on the same dot (excitation represented by a straight line), and four CT, i.e., h1A-eB (CT states; *Bottom*), where the hole and the electron are localized on different dots (excitation represented by a curved line). (*C*) Eigenexciton states of a heterodimer QD_A–QD_B with $\overline{D}_A = 2.4$ nm and $\overline{D}_B = 3.6$ nm and a dot separation (surface to surface distance) L = 0.55 nm. The eigenexcitons can be designated by their zero-order label because the intradot and interdot Coulomb interactions are weak. In an ensemble of size-dispersed dimers, each level in *C* is the mean value of an energy distribution that for moderate size dispersion (up to 5% in diameter) remains Gaussian; see *SI Appendix*, sections S1 and S2, and ref. 47 for additional details, validation of the energy levels model, and figures.

determinants that allow for a single excitation. These are the zeroth-order exciton states. We start with a single electron description for three one-particle states of each dot. As shown in Fig. 1*B*, in the dimer the excitation can either be localized on the same dot, either dot A (h1eA and h2eA) or dot B (h1eB and h2eB), leading to four local (Frenkel) excitons, two on each dot, or involve the two dots, leading to four CT states (h1AeB, h2AeB, h1BeA, and h2BeA).

To go beyond an independent particle model we add coulombic and exchange coupling within (intradot) and between the dots (interdot). The interdot Coulomb coupling magnitude depends also on the distance between the dots. Both types of Coulomb coupling are typically weak: the intradot Coulomb coupling because of the rather large energy differences between the excitons of the isolated dots (*SI Appendix*, Fig. S1) and the interdot ones because of the surface to surface distance. Diagonalization of the two-particle Hamiltonian results in the eight eigenstates of the dimer shown in Fig. 1*C*. See *SI Appendix*, section S1, model excitonic Hamiltonian, and ref. 47 for additional details. The level structure of the eigenstates shown in Fig. 1*C* is computed for a dot separation of 0.55 nm and dot diameters $\overline{D}_A = 2.4$ nm and $\overline{D}_B = 3.6$ nm.

To label the eigenstates of dimers of different size we use the index α. It is a two-digit index because it specifies the size of each one of the two dots in the dimer. Note that also in a nominally homodimer for which the two dots have the same mean size, the two dots need not be exactly of the same size because of the size dispersion. In a heterodimer as shown in Fig. 1 the two dots are of different mean size. The label α suffices also after including the coupling of two monomers because we take it that the different dimers are sufficiently far apart to be weakly interacting.

By sampling independently 4,000 dots with a Gaussian size distribution of 5% in diameter we get the dispersion in energies in an ensemble of single dots as shown in *SI Appendix*, Fig. S1. Shown in *SI Appendix*, Fig. S2, is the generated distribution of eigenenergies in an ensemble of 4,000 dimers. Shown also is a fit for the energies of each state to a Gaussian distribution; see *SI Appendix*, Tables S1 and S2, for values of the parameters. It follows from the results shown in *SI Appendix*, Fig. S2, and our other simulations that the higher excited states often have a wider width in their energy spacings to other states. The distribution of size-dependent properties that is of direct relevance to our computation is that of differences between eigenstate energies. Taking the energies to be Gaussian distributed allows an analytical computation of the distribution of their difference that will also be Gaussian, with a width that depends on the extent of correlation between the two levels (*SI Appendix*, Figs. S3 and S4 and Tables S3 and S4). When higher excited states are involved, the Gaussian distribution of the energy differences can be distorted, and higher moments may be needed to characterize the distribution of the energy spacings as discussed in *SI Appendix*, section S2.

The Dynamics of Observables

The dimers in the array are sufficiently far apart so that they are effectively not interacting. Thereby the array is an ensemble of independent dimers. The group structure underlying the dynamics of an isolated dimer is discussed in this section. It is this structure that enables the parallelism in the information processing. Each dimer has a ground state (GS) and a set of eight orthonormal quantum excitonic states listed in Fig. 1*B* and shown explicitly in Fig. 1*C*. This means that all quantum mechanical operators for the model can be represented as 9×9 Hermitian matrices. We label the basis states of the matrices $|n\rangle$, $n = 0,1,2,..,N$. $n = 8$ in the example we use, and $n = 0$ is to the GS. A dimer is indexed by its size parameters $\boldsymbol{\alpha}$, and later we will average over the distribution of $\boldsymbol{\alpha}$. In this section we focus on a single dimer, and $\boldsymbol{\alpha}$ has a constant given value. For any value of α the Hamiltonian is a 9×9 matrix where the entries are functions of the size index. The elements of the density matrix of a dimer will also depend on the size.

The Hamiltonian $H_{\boldsymbol{\alpha}}$ of dimer of size $\boldsymbol{\alpha}$ consists of three kinds of terms. Diagonal terms are the energies of the zeroth-order excitonic states. Off-diagonal terms mix the states by two quite different mechanisms. One kind is due to the hole electron Coulombic and exchange interactions, and the other kind is the dipole coupling of states induced by the pumping lasers. We do not assume that the coupling by the lasers is weak so that multiphoton transitions are possible, but we do assume that the lasers are not intense enough to access higher excited states of the dots that are not in our basis. It is useful to diagonalize the Coulombic and exchange interactions. This will be referred to as the eigenstates basis. In this basis the Hamiltonian is diagonal when the laser is off.

We write the Hamiltonian of a dimer of size $\boldsymbol{\alpha}$ as a 9×9 matrix in the space of the accessible states

$$\begin{aligned} H_{\boldsymbol{\alpha}} &= \sum_{n,m} h_{\boldsymbol{\alpha}}^{nm} |n\rangle\langle m| \\ &= \sum_{n,m} h_{\boldsymbol{\alpha}}^{nm} E_{nm}. \end{aligned} \quad [1]$$

It is convenient already here to introduce the notation $E_{nm} \equiv |n\rangle\langle m|$. The coherences E_{nm} have a very useful representation as an $N \times N$ matrix where all of the elements are zero except for the number 1 in the position n, m. It is appropriate to refer to these as Gelfand matrices (48, 49).

In the eigenstate basis and when the laser is not strong, the diagonal matrix elements are the eigenenergies. The off-diagonal matrix elements are the dipole transitions induced by the laser. These elements are time dependent. After the laser pulses are over, the Hamiltonian is diagonal, and only the phase of the eigenstates changes in time.

Each dimer is coherently pumped, and so, starting from the GS, each dimer can be described by a wave function. The wave function for dimer α at the time t is of the form $|\psi_\alpha(t)\rangle = \sum_m C_{\alpha m}(t)|m\rangle$, where the coefficients $C_{\alpha m}(t)$ are arranged as a column vector. When initially (time = 0) the dimers are in their GS, all of the $C_{\alpha m}(t = 0)$ coefficients are zero except for $C_{\alpha 0}$. Otherwise the coefficients vary with time due to the laser pulses. The density matrix of a dimer of size $\boldsymbol{\alpha}$ is $|\psi_\alpha(t)\rangle\langle\psi_\alpha(t)| = \sum_{mn} C_{\alpha m}(t) C^*_{\alpha n}(t)|m\rangle\langle n|$. Using the notation $E_{mn} \equiv |m\rangle\langle n|$ for the coherences (or the populations for $m = n$), the density matrix for any given dimer can be written as

$$\boldsymbol{\rho}_{\boldsymbol{\alpha}}(t) = \sum_{mn} \boldsymbol{\rho}_{\boldsymbol{\alpha}}^{mn}(t) E_{mn}, \quad [2]$$

where the coherence for a given size α is

$$\boldsymbol{\rho}_{\boldsymbol{\alpha}}^{mn}(t) = C_{\boldsymbol{\alpha}m}(t) C^*_{\boldsymbol{\alpha}n}(t) = \mathrm{Tr}\left(\boldsymbol{\rho}_{\boldsymbol{\alpha}} E_{nm}\right) \equiv \langle E_{nm}\rangle. \quad [3]$$

The Gelfand matrices satisfy the commutation relation

$$[E_{nm}, E_{kl}] = \boldsymbol{\delta}_{m,k} E_{nl} - \boldsymbol{\delta}_{l,n} E_{km} \quad [4]$$

of the Lie algebraic Unitary group (49) U(N).

The Hamiltonian (Eq. **1**) and the density matrix (Eq. **2**) are linear sums of the Gelfand matrices. Moreover, the commutator of two such matrices (Eq. **4**) is also linear in the matrices. Any observable of the system of N levels and, in particular, the density matrix and its time evolution can be fully specified as a linear combination of the Gelfand matrices with time-dependent coefficients. It can also be proven for other algebras (50) by using the Liouville equation of motion for the density matrix. The

closure property (Eq. **4**) and when the Hamiltonian is linear in the coherences (Eq. **1**) imply that the values of the coefficients $C_{\alpha m}(t)$ as a function of time satisfy a first-order in time linear differential equation. The Heisenberg equation of motion for the mn matrix E_{nm} is

$$\begin{aligned} i\hbar\frac{\partial}{\partial t}E_{nm} &= [E_{nm}, H_\alpha] = \sum_{kl} h_\alpha^{kl}[E_{nm}, E_{kl}] \\ &= \sum_{kl} h_\alpha^{kl}\left(\delta_{m,k}E_{nl} - \delta_{l,n}E_{km}\right) \\ &= \sum_l h_\alpha^{ml}E_{nl} - \sum_k h_\alpha^{kn}E_{km}. \end{aligned} \quad [5]$$

In terms of the elements of the density matrix, $\boldsymbol{\rho}_{\boldsymbol{\alpha}}^{mn}(t) = \langle E_{nm}(\boldsymbol{\alpha})\rangle$, this closure reads

$$i\hbar\frac{\partial}{\partial t}\rho_\alpha^{mn} = \sum_l h_\alpha^{ml}\rho_\alpha^{ln} - \sum_k h_\alpha^{kn}\rho_\alpha^{mk}. \quad [6]$$

For computational purposes it is convenient to arrange the density matrix elements as a vector of length N^2 by listing its indices in a lexicographical order. Then the equation of motion of the N^2 observables is a Liouvillian matrix acting on a vector

$$i\hbar\frac{\partial}{\partial t}\rho_\alpha^{mn} = \sum_{kl} L_{mn,kl}\rho_\alpha^{kl}. \quad [7]$$

Eqs. **6** and **7** describe the time evolution of the elements of a density matrix of a dimer of size. The equations determine the value of N2 variables [N populations (that sum up to unity) and $N(N-1)$ coherences]. The role of the device is to produce the values of the N^2 variables after the laser pulse is over, and the equations of motion **6** and **7** can be solved to provide these values for a dot of a particular size. The point we ask to make here is that the solution of the equations of motion exhibits parallelism. To show this we note that the N^2 by N^2 Liouvillian matrix can be diagonalized. Each eigenvector is an independent mode of motion. There will be N^2 eigenvalues, at least one of which will be zero (= the conservation of probability) at the level of a dimer of a given size. By writing each element of the density matrix as a sum over eigenvectors of the Liouvillian matrix it follows that each such value can be reached by up to N^2-1 distinct pathways, which is the maximal number of nonzero eigenvalues of the Liouvillian matrix (see, for example, refs. 51 and 52). This parallelism is a direct outcome of the linearity of quantum dynamics as expressed in Eq. **5**. The parallelism is an essential ingredient in our approach, and one key purpose of this paper is to show that the parallelism is maintained also when we need to average over a distribution of sizes of the dots, provided that distribution is not too broad (in a sense to be defined).

Eqs. **6** and **7** exhibit parallelism at the level of a dimer of a given size. The role of the device is to produce the values of the N^2-1 variables [$N-1$ populations (that sum up to unity) and $N(N-1)$ coherences] after the laser pulse is over. By diagonalizing Eq. **7** it is shown that each such value can be reached by up to N^2-1 distinct pathways which is the maximal number of nonzero eigenvalues of the Liouvillian matrix. See, for example refs. 51 and 52. Each pathway is an eigenvector of the Liouvillian matrix. This parallelism is a direct outcome of the linearity of quantum dynamics as expressed in Eq. **5**.

The Liouvillian matrix, made up by the elements of the Hamiltonian, is relatively sparse. The off-diagonal elements of the Hamiltonian are time dependent because of the laser pulses connecting different states of the dimer. After the pulses are over, the Hamiltonian is purely diagonal, and the equations of motion have the far simpler form

$$i\hbar\frac{\partial}{\partial t}\rho_\alpha^{mn}(t) \xrightarrow{\text{after the addressing}} \left(h_\alpha^{mm} - h_\alpha^{nn}\right)\rho_\alpha^{mn}(t), \quad [8]$$

meaning that after the pulses the coherences oscillate with frequencies given by the transition frequencies of the two corresponding states.

The Dynamics of the Ensemble

Next we need to perform an average over an ensemble (= mixture) of noninteracting dimers that differ somewhat in their size. The straightforward way of doing so is to solve the equation of motion for every dimer of size α and at any time t of interest to perform an averaging of the coherences $\rho_\alpha^{mn}(t)$ over the size distribution

$$\boldsymbol{\rho}^{nm}(t) = \sum_{\boldsymbol{\alpha}} p_{\boldsymbol{\alpha}}\boldsymbol{\rho}_{\boldsymbol{\alpha}}^{nm}(t). \quad [9]$$

Here p_α is the probability of a dimer of size α in the mixture. The density matrix of the mixture, $\boldsymbol{\rho} = \sum_{\boldsymbol{\alpha}}|\boldsymbol{\alpha}\rangle p_{\boldsymbol{\alpha}}\boldsymbol{\rho}_{\boldsymbol{\alpha}}\langle\boldsymbol{\alpha}|$, is also diagonal in the size index where we take dimers of different size to be distinct, $\langle\alpha'|\alpha\rangle = \delta_{\alpha'\alpha}$. To identify the Hamiltonian H that acts to propagate in time the density matrix of the ensemble we impose that each dimer evolves independently of the others,

$$i\frac{d}{dt}\boldsymbol{\rho} = \sum_{\boldsymbol{\alpha}}|\boldsymbol{\alpha}\rangle p_{\boldsymbol{\alpha}} i\frac{d}{dt}\boldsymbol{\rho}_{\boldsymbol{\alpha}}\langle\boldsymbol{\alpha}| = \sum_{\boldsymbol{\alpha}}|\boldsymbol{\alpha}\rangle p_{\boldsymbol{\alpha}}\left[H_{\boldsymbol{\alpha}}, \boldsymbol{\rho}_{\boldsymbol{\alpha}}\right]\langle\alpha|. \quad [10]$$

It follows that for dimers that are not interacting, the Hamiltonian H that is the generator of the motion of the mixture is diagonal in the index α:

$$\begin{aligned} H &= \sum_{\boldsymbol{\alpha}}|\boldsymbol{\alpha}\rangle H_{\boldsymbol{\alpha}}\langle\boldsymbol{\alpha}| \\ &= \sum_{\boldsymbol{\alpha}}|\boldsymbol{\alpha}\rangle\sum_{nm} h_{\boldsymbol{\alpha}}^{nm}E_{nm}(\boldsymbol{\alpha})\langle\boldsymbol{\alpha}| \\ H_{\boldsymbol{\alpha}} &= \sum_{nm} h_{\boldsymbol{\alpha}}^{nm}E_{nm}(\boldsymbol{\alpha}). \end{aligned} \quad [11]$$

The Hamiltonian H generates the coherent motion of the averaged coherences. Note that after the pulse the averaged Hamiltonian H is diagonal because the Hamiltonian of each dimer is diagonal.

There is, however, a key difference brought about by the need to average. The equations of motion (Eq. **6**) for the coherence of a particular dimer are closed. However, the equations of motion for the coherence averaged over the dimers are not closed:

$$\begin{aligned} i\frac{\partial\boldsymbol{\rho}^{nm}}{\partial t} &= \sum_{\boldsymbol{\alpha}} p_{\boldsymbol{\alpha}}\left(i\frac{\partial}{\partial t}\boldsymbol{\rho}_{\boldsymbol{\alpha}}^{nm}\right) = \sum_{\boldsymbol{\alpha}} p_{\boldsymbol{\alpha}}\sum_{kl} h_{\boldsymbol{\alpha}}^{kl}\left(\boldsymbol{\delta}_{nk}\boldsymbol{\rho}_{\boldsymbol{\alpha}}^{lm} - \boldsymbol{\delta}_{lm}\boldsymbol{\rho}_{\boldsymbol{\alpha}}^{nk}\right) \\ &= \sum_{\boldsymbol{\alpha}} p_{\boldsymbol{\alpha}}\sum_l h_{\boldsymbol{\alpha}}^{nl}\left(\boldsymbol{\rho}_{\boldsymbol{\alpha}}^{lm}\right) - \sum_{\boldsymbol{\alpha}} p_{\boldsymbol{\alpha}}\sum_k h_{\boldsymbol{\alpha}}^{km}\left(\boldsymbol{\rho}_{\boldsymbol{\alpha}}^{nk}\right). \end{aligned} \quad [12]$$

The problem arises because the averaging over the different sizes and the time propagation do not commute, technically because the Hamiltonian of the dimer depends on the size. The coherences of different dimers will therefore oscillate with different frequencies. In an N-level system, there are N^2 observables, so to converge the average of each requires computing a large number of samples meaning that sampling over the size distribution is a reliable but a rather tedious route.

Computing the proper ensemble average requires very many repetitions of solving N coupled first-order in time differential equations. Our aim below is to numerically simplify this task. It is important to note that this exact result maintains the parallelism as discussed for a single dimer following Eq. **7**. That the parallelism is maintained is to be expected because we are averaging over independent dimers. What we seek to do next is to avoid the need to average over many independent repetitions of the dynamics.

A quantum mechanical ensemble will evolve coherently if it evolves under a given Hamiltonian. With foresight we adopt the averaged Hamiltonian H as given in Eq. **11**. This is because, as we discuss below, the frequency of the coherence when averaged over the dots, $\boldsymbol{\rho}^{nm}(t)$ of Eq. **12**, is the same as the frequency of the coherence computed for a coherent evolution generated by the averaged Hamiltonian. We shall also show computational examples for this analytical result.

We denoted by ρ_c the density matrix for the same set of states as in the ensemble$\rho_c(t) = \sum_{ij}\rho_c^{ij}(t)E_{ij}$. This density is defined such that it is propagated in time quantum mechanically under the averaged Hamiltonian $H = \sum_{kl}H_{kl}E_{kl}$ (Eq. **11**). Since both ρ_c and H are linear combination of operators that are in the algebra, it means that the equations of motion for the coherences, $\boldsymbol{\rho}_c^{mn}$, are closed.

$$i\frac{\partial\boldsymbol{\rho}_c^{nm}}{\partial t} = \left(\sum_k H_{km}\boldsymbol{\rho}_c^{nk} - \sum_l H_{nl}\boldsymbol{\rho}_c^{ml}\right). \quad [13]$$

The closure property of the algebra (Eq. **4**) leads immediately to this result.

It follows that we can solve the equations of motion for the coherences, and we chose initial conditions such that ρ_c and the density matrix of the averaged ensemble (Eq. **12**) coincide at the initial time.

To generate a fully coherent time evolution, one can average first over the size dispersion and only then generate the motion. This is a tremendous savings in computational effort. It is therefore of much practical interest to achieve the same compaction for the motion of the coherence in the real ensemble which is a mixture.

After the pulse the Hamiltonian is diagonal, and the coherences of $\boldsymbol{\rho}_c$ evolve periodically:

$$i\frac{\partial\rho_c^{nm}}{\partial t} = (H_{mm} - H_{nn})\rho_c^{nm}. \quad [14]$$

We define a time T such that the effective excitation by the pulse is over. We find that taking T to be a time just past the maximum of the envelope of the field works best. For any time t later than T,

$$\rho_\alpha^{nn}(t) = \exp(-i(h_\alpha^{mm} - h_\alpha^{nn})(t-T))\rho_\alpha^{nn}(T). \quad [15]$$

Performing an averaging of the coherences over the size distribution leads to

$$\begin{aligned}\boldsymbol{\rho}^{nm}(t) &= \sum_\alpha p_\alpha\boldsymbol{\rho}_\alpha^{nm}(t)\\ &= \sum_\alpha p_\alpha\exp(-i(h_\alpha^{mm} - h_\alpha^{nn})(t-T))\boldsymbol{\rho}_\alpha^{nm}(T).\end{aligned} \quad [16]$$

Here enters our approximation. For the time T of the pulse we will approximate $\boldsymbol{\rho}^{nm}(T)$ by $\boldsymbol{\rho}_c^{nm}$. Numerically, it is a close approximation, and we shall show that it is valid as long as the dephasing during the pulse is negligible, which requires that the time T is short compared to the shortest dephasing time, which we calculate below. Then

$$\begin{aligned}\rho^{nm}(T) &= \sum_\alpha p_\alpha\rho_\alpha^{nm}(T) \simeq \rho_c^{nm}(T)\\ \rho^{nm}(t) &= \sum_\alpha p_\alpha\exp(-i(h_\alpha^{mm} - h_\alpha^{nn})(t-T))\rho_\alpha^{nm}(T)\\ &= \left\{\sum_\alpha p_\alpha\exp(-i(h_\alpha^{mm} - h_\alpha^{nn})(t-T))\right\}\rho_c^{nm}(T).\end{aligned} \quad [17]$$

The averaging is analytically approximated using a cumulant expansion over a random variable X (53, 54),

$$\ln\langle\exp(itX)\rangle = \mu it - \left(\frac{\sigma^2}{2}\right)t^2 - i\frac{\kappa_3}{3!}t^3 + \frac{\kappa_4}{4!}t^4 + \ldots \quad [18]$$

Here μ and σ^2 are the variance, and κ_3 and κ_4 are the third and fourth cumulants of X (*SI Appendix*, section S3). To leading order,

$$\begin{aligned}\boldsymbol{\rho}^{nm}(t) &\simeq \left\{\sum_\alpha p_\alpha\exp(-i(h_\alpha^{mm} - h_\alpha^{nn})(t-T))\right\}\boldsymbol{\rho}_c^{nm}(T)\\ &\approx \exp(-i\boldsymbol{\varpi}_{mn}(t-T))\exp(-(\boldsymbol{\sigma}_{mn}^2/2)(t-T)^2)\boldsymbol{\rho}_c^{nm}(T).\end{aligned} \quad [19]$$

Here $\boldsymbol{\varpi}_{mn}$ is the mean frequency of the nm coherence

$$\boldsymbol{\varpi}_{mn} = \sum_\alpha p_\alpha(h_\alpha^{mm} - h_\alpha^{nn}), \quad [20]$$

and it has the same value as the frequency of the coherence $\boldsymbol{\rho}_c^{mn}(t)$ generated by the averaged Hamiltonian. $\boldsymbol{\sigma}_{mn}^2$ is the variance

$$\boldsymbol{\sigma}_{mn}^2 = \sum_\alpha p_\alpha(h_\alpha^{mm} - h_\alpha^{nn})^2 - \boldsymbol{\varpi}_{mn}^2. \quad [21]$$

As long as $(\boldsymbol{\sigma}^{mn}T/\sqrt{2})^2 < 1$, there is not much dephasing during the pulse, and Eq. **19** can be a good approximation. It further follows that as long as $(\boldsymbol{\sigma}_{mn}T/\sqrt{2})^2 < 1$ is valid, the approximation is not going to be very sensitive to the precise value of T.

The cumulant expansion (Eq. **18**) contains higher terms beyond the second. These are the third and beyond cumulants of the distribution of the frequencies of a coherence where the distribution is due to the size dispersion which means that the eigenenergies h_α^{mm} and h_α^{nn} depend on the size α. The computational results are that most of the distributions of energy differences are close to Gaussian (*SI Appendix*, Figs. S1– S4 and sections S2 and S3). For a Gaussian distribution, all of the cumulants beyond the second vanish. This implies that for the distribution of energy differences the cumulants beyond the second are essentially negligible. The third cumulant is a measure of the skewness of the distribution, and it is seen by inspection that the actual distribution is typically symmetric about its mean. The fourth cumulant is a measure called "excess" or "kurtosis." It shows how much the tails of the distribution are deviant from that of a Gaussian. So also for the fourth cumulant the tight fit to a Gaussian distribution shows that for most of the energy difference distributions, the first two cumulants suffice. In the numerical examples discussed below, the distribution of the frequencies of some coherences that involve pairs of eigenstates that go through an avoided crossing as a function of the sizes of the two dots that constitute the dimer (*SI Appendix*, Figs. S5 and S7) cannot be fitted by a Gaussian distribution. This is expected from the general theory because the index α that designates the pair of dot sizes is no longer a good label; for further details, see *SI Appendix*, section S2.

The result of Eq. **19** is based on propagating with an averaged Hamiltonian and then superposing dephasing. Equivalently, one can introduce an averaged Liouvillian in which the dephasing can be built in directly in the Liouvillian. This is discussed explicitly in *SI Appendix*, section S4.

Results

We compare the dynamics of the coherences in a dimer computed by performing explicitly the ensemble average of the dynamics of $N_d = 4{,}000$ dimers as given by the first two lines of Eq. **12** that we call in this section $\rho_{av}^{nm}(t)$,

$$i\frac{\partial\boldsymbol{\rho}_{av}^{nm}(t)}{\partial t} = (1/N_d)\sum_\alpha\left[\sum_{l=0}^{N}h_\alpha^{nl}(t)\boldsymbol{\rho}_\alpha^{lm}(t) - \sum_{k=0}^{N}h_\alpha^{km}(t)\boldsymbol{\rho}_\alpha^{nk}(t)\right], \quad [22]$$

with the approximate dynamics computed using Eq. **19** where we include the first three cumulants,

$$\rho_{ens}^{nm}(t) = \exp\Big(-i\varpi_{mn}(t-T) - i\frac{\kappa_3}{6}(t-T)^3\Big)\exp\Big(-\sigma_{mn}^2\frac{(t-T)^2}{2}\Big)\rho_c^{nm}(T), \quad [23]$$

where $\rho_c^{nm}(t)$ is propagated with the average Hamiltonian, H, using Eq. **14**. ϖ_{mn} and σ_{mn}^2 are the average frequency and variance over the ensemble given by Eqs. **20** and **21**, respectively, and κ_3 is the third cumulant (53) (*SI Appendix*, section S4). We do not include the fourth cumulant because it cannot be fully accurately computed due to the limitation of a finite sampling. We show that the agreement between the two dynamics is excellent to good, depending on how close the distribution of coherence frequencies is to a Gaussian distribution. As can be seen from Figs. 2 and 3 below, only slow beating coherences with more distorted frequency distribution are somewhat less well described by the ensemble propagation. This very good agreement shows that the algebraic approach to the dynamics of the ensemble discussed in *SI Appendix*, section 4, and the working expression given by Eq. **23** capture the essence of the role of size disorder in arrays of QD dimers. The algebraic structure is preserved at the level of the disordered ensemble. This allows processing information in parallel by addressing and reading the N^2 coherences of a classical ensemble of dimers with realistic size dispersion. The dephasing times computed for 5% size dispersion are of the order of 20 to 30 fs or less for coherences involving the GS and up to 100 fs for coherences between excited states, which makes our conclusion also valid for room temperature experiments where $1/kT = 26$ fs. When a tighter size dispersion will be experimentally achievable, this conclusion will be even stronger.

To illustrate this conclusion, we consider ensembles of two types of dimers, the heterodimer whose level structure is shown in Fig. 1*C* ($\overline{D}_A = 2.4$ nm and $\overline{D}_B = 3.6$ nm) and a quasi-homodimer with $\overline{D}_A = 3.4$ nm and $\overline{D}_B = 2.4$ nm whose level structure is shown in *SI Appendix*, Fig. S7 and section S2. For both ensembles, the size dispersion is Gaussian with a realistic variance of 5% in diameter (half width at half maximum = 5.8%) as shown in Fig. 1*A* for the heterodimer ensemble.

The ensembles of dimers are excited by a short few-cycle visible (Vis) fs pulse. The oscillations of the electric field of the pulse are confined in a Gaussian envelope whose duration ($\sigma_{nm} = 1.41$ fs, full width at half maximum [FWHM] = 3.32 fs, FWHM in energy of 1.1 eV) is shorter than most of the dephasing times, σ_{nm} (Eq. **21**), of the distributions of the frequencies of the coherences. The carrier frequency of the pulse is tuned to be resonant with the bright excitonic bands: $\omega = 2.50$ eV for the heterodimer ensemble and $\omega = 2.56$ eV for the ensemble of quasi-homodimers. For both pulses, the field strength is 0.0002 a.u. which corresponds to a peak intensity of $1.4\ 10^9$ W/cm^2, and the maximum of the pulse envelope occurs at 24.1 fs.

In the case of the heterodimer ensemble, the pulse accesses essentially the two bands of local exciton eigenstates resonant with the pulse, h2eB and h1eA, which are slightly mixed and overlapping (*SI Appendix*, Fig. S2). The population of the h2eB band (mean energy of 2.52 eV) which is the brightest is 4.5%,

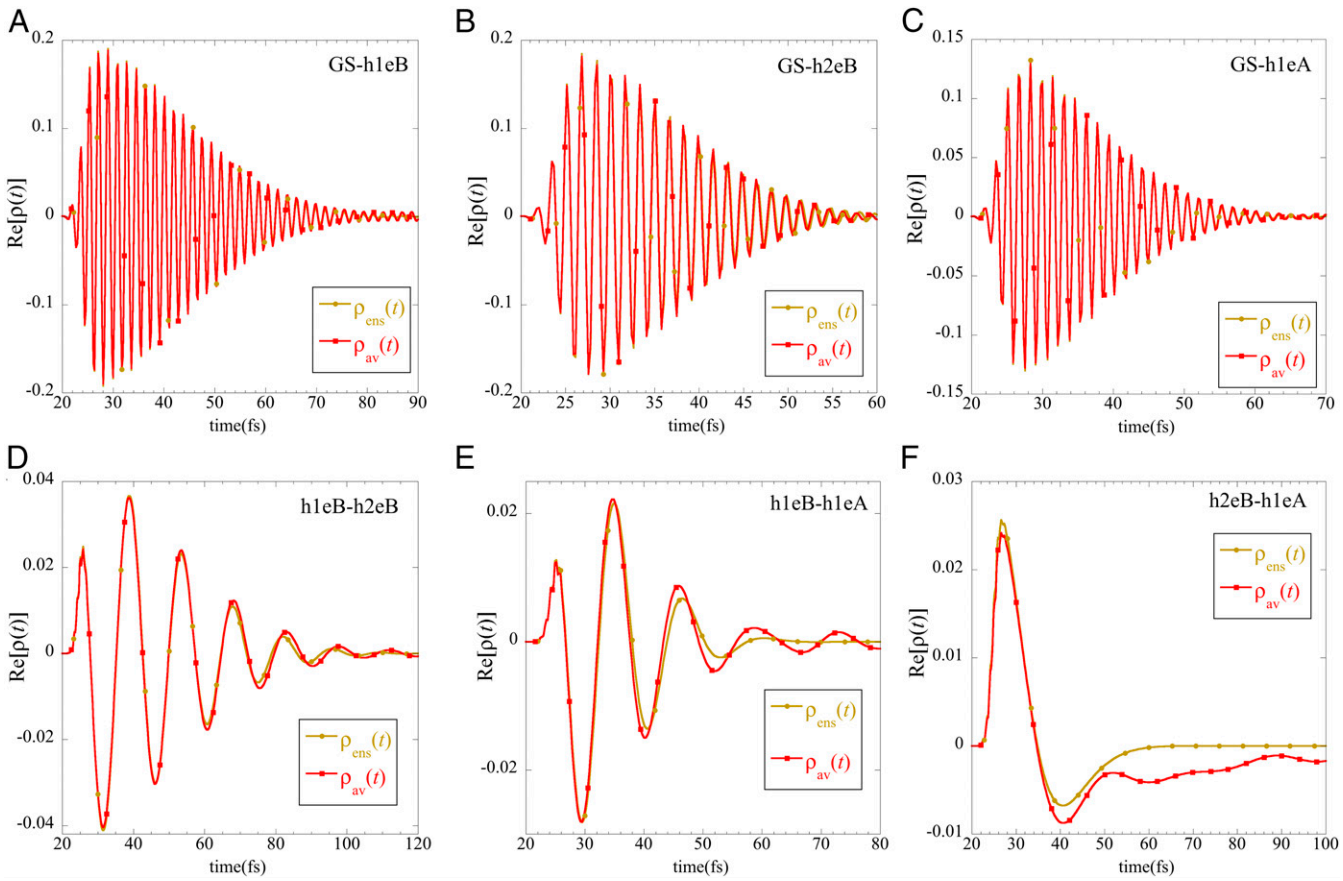

Fig. 2. Comparison of the coherence dynamics computed by a single integration of $\rho_{ens}^{nm}(t)$ (Eq. **23**; golden lines with circles) and $\rho_{av}^{nm}(t)$ (Eq. **22**) by averaging the individual time evolution of the 4,000 heterodimers ($\overline{D}_A = 2.4$ nm, $\overline{D}_B = 3.6$ nm, 5% dispersion in diameter) of the ensemble. The dynamics of coherences from the GS to the local excitons h1eB, h2eB and h1eA is shown in panels *A*, *B*, and *D*, respectively. The dynamics of coherences between excitons (h1eB-h2eB, h1eB-h1eA and h2eB-h1eA) is shown in panels *D*, *E*, and *F*. The first three cumulants are included in Eq. **23**. The values of all of the cumulants of the frequency distributions of the six coherences are reported in *SI Appendix*, Table S5, up to fourth order, and the frequency distributions are shown in *SI Appendix*, Figs. S2 and S3 and section S2.

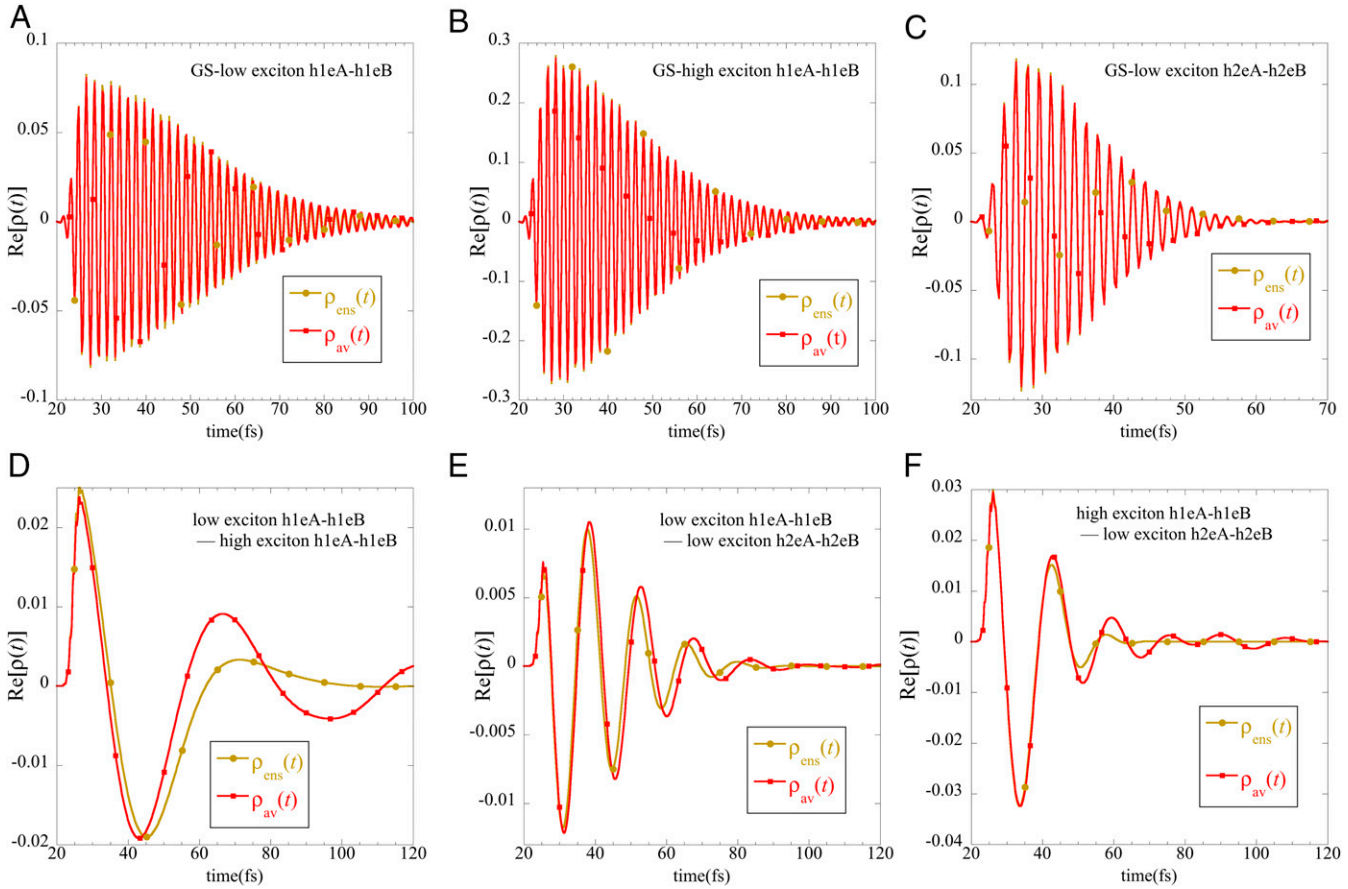

Fig. 3. Comparison of the coherence dynamics computed by a single integration of $\rho_{ens}^{nm}(t)$ (Eq. **23**; golden lines with circles) and $\rho_{av}^{nm}(t)$ (Eq. **22**) by averaging the individual time evolution of the 4,000 quasi-homodimers ($\overline{D}_A$ = 3.4 nm, $\overline{D}_B$ = 3.6 nm, 5% dispersion in diameter) of the ensemble. The dynamics of coherences from the GS to selected excitons is shown in panels *A*, *B*, and *D*. The dynamics of coherences between selected pairs of excitons is shown in panels *D*, *E*, and *F*. The first three cumulants are included in Eq. **23**. The values of all of the cumulants of the frequency distributions of the six coherences are reported in *SI Appendix*, Table S7, and the frequency distributions are shown in *SI Appendix*, Figs. S2 and S3.

and there is 2.35% population in the slightly higher in energy h1eA band, centered at 2.62 eV. The excitonic band h1eB which lies on the low side of the laser bandwidth (at 2.24 eV) has a population of 4.29%. CT excitonic bands have very low oscillators, and their populations are lower than 10^{-2}%. The population in the higher local excitonic band h2eA is lower than 0.1%. We show in Fig. 2 *A–C* the comparison of the dynamics of the three fast beating (periods of the order of 1.5 fs) and fast dephasing (dephasing times σ_{nm} of the order of 25 to 30 fs; *SI Appendix*, Table S1) GS-h1eB, GS-h2eB, and GS-h1eA electronic coherences, computed as an ensemble average (Eq. **22**) and using the approximation of ρ_{ens} given in Eq. **22**. The agreement is excellent, and the results of both dynamics are almost indistinguishable. Fig. 2 *D–F* shows the time evolution of coherences between excited states: h1eB–h2eB intradot electronic coherence (Fig. 2*D*) and two interdot electronic coherences, h1eB–h1eBA and h2eB–h1eA (Fig. 2 *D* and *E*). The periods of the h1eB–h2eB and h1eB–h1eA coherences are more than one order of magnitude slower than the fast beating ones of Fig. 2 *A–C*. Their dephasing times are comparable or longer depending on the correlation between the pair of energy level distributions involved; see *SI Appendix*, section S2, for a discussion and for the values of the dephasing times. For these two coherences, the agreement between the two approaches is also very good, and they exhibit enough oscillations within their dephasing envelope to be measurable by 2D electronic spectroscopy. However, the interdot coherence h2eB–h1eA (Fig. 2*F*) dephases too quickly to be experimentally observed and is equally not useful for logic processing. As discussed above and in *SI Appendix*, section S2, this coherence involves a pair of eigenstates that go through an avoided crossing as a function of the sizes of the two dots that constitute the dimers (*SI Appendix*, Fig. S5). In that case, one does not expect theρ_{ens} approach to be valid, and the distribution of the energy differences between these two eigenstates is not Gaussian (*SI Appendix*, Fig. S3). This coherence exhibits a complex behavior with several periods and dephasing times. The dephasing rate could be corrected by adding higher cumulants in Eq. **23**. However, their values are not stable for the 4,000-dimer ensemble considered here.

We next turn to the case of the ensemble of quasi-homodimers, for which there is an almost complete overlap of the zero-order exciton bands, leading to eigenexcitons delocalized over the two dots. A representative scheme of the level structure of a single dimer is shown in *SI Appendix*, Fig. S6. Within a single quasi-homodimer, the coupling between two quasi-degenerate zero-order excitons leads to a lower and to a higher eigenstate delocalized over the two dots, roughly separated in energy by twice the coupling strength. The interdot Coulomb coupling is the strongest between local excitons. It is much weaker between CT states. Since there are two local excitons per dot, we get four mixed eigenstates made of local excitons and four mixed CT states. The four eigenstates made by the coupling of local excitons carry essentially all of the oscillator strength. We label them low exciton h1eA–h1eB, high exciton

h1eA–h1eB, low exciton h2eA–h2eB, and high exciton h2eA–h2eB (*SI Appendix*, Fig. S6). At the level of the ensemble, we get eigenexciton bands of mixed nature, delocalized over the two dots. Among them, the pulse accesses the lowest three local bands: low exciton h1eA–h1eB, high exciton h1eA–h1eB, and low exciton h2eA–h2eB. In the case of the homodimer ensemble, all of the coherences have an interdot character.

We show the six coherences resulting from the population of these three eigenexciton bands by the pulse in Fig. 3. As in the case of the ensemble of heterodimers, the dynamics of GS–exciton coherences (Fig. 3 *A*–*C*) and of the rather fast beating coherences between excited states shown in Fig. 3 *E* and *F* are very well captured by the propagation of the $\rho_{ens}(t)$ density matrix (Eq. **23**). The very slow beating coherence between low/high exciton h1eA–h1eB (Fig. 3*D*) is less well captured. The reason is the same as for the coherence shown in Fig. 2*F* in the case of the ensemble of heterodimers. This pair of dimer states goes through an avoided crossing as a function of the sizes of the two dots of the dimer (*SI Appendix*, Fig. S7), and one does not expect the ρ_{ens} approach to be valid. This quickly dephasing coherence will, however, be difficult to observe experimentally because of its low intensity and of the few oscillations of different periods that occur before its complete dephasing. As was the case for the slow beating coherence of the heterodimer (Fig. 2*D*), such coherences cannot be used to encode and process information in a logic scheme. Because of their slower beating periods and multi-dephasing times, they are also more likely to interact with phonons and be subject to environmental perturbations.

We show in *SI Appendix*, Figs. S8 and S9 and section S4, the dynamics of the same coherences as in Figs. 2 and 3 but computed for a narrower 3% size dispersion. The dephasing rates are 2 to 3 times slower than for 5% size dispersion ensembles, and the fits to Gaussian distributions are tighter (*SI Appendix*, Figs. S2 and S4 and Tables S2, S4, S6 and S8). As expected, narrower size dispersions are beneficial and make the ρ_{ens} approach even more accurate, except for the coherences of *SI Appendix*, Figs. S8*F* and S9*D*, which correspond to pairs of states undergoing an avoided crossing as a function of dot size. For those coherences, reducing the size dispersion is not beneficial.

In conclusion, we showed that as a practical proposition the inevitable size dispersion of ensembles of colloidal QDs means that somewhat fewer than N^2 logic variables are available for information processing in an N state quantum device. The coherences that are not useful are rather slow beating and would be hard to read because of their rather fast Gaussian dephasing in time. Except for the very slow beating ones the dephasing of the coherences could be well captured by the two lowest cumulants of the spacing distributions. These cumulants can, of course, be computed directly from the eigenvalues determined by diagonalizing the Hamiltonian and do not require computing the temporal evolution. It is the second cumulant, the width of the spacing distribution, that is the width of the Gaussian dephasing in time. The third and fourth cumulants allow for a fine matching of the dephasing as computed by averaging the dynamics over the ensemble. The faster beating coherences are expected to be more resilient both to thermal fluctuations and to dynamical coupling to interdot and intradot vibrations. A point about the addressing lasers is that the most resilient faster beating coherences, those most suitable for information processing, could dephase too fast for them to be detected if the pumping is not fast enough. In typical 2D electronic spectroscopy the pump is fast enough so that its frequency profile spans broad swaths of the absorption spectrum, but this may not always be fast enough to allow detection of the fast dephasing due to extreme size dispersion.

Data Availability. There are no data underlying this work.

ACKNOWLEDGMENTS. This work is supported by the Future Emerging Technologies open European Commission project COPAC 766563 and the Fonds National de la Recherche Scientifique (FRS-FNRS; Belgium), T.0205.20. Computational resources have been provided by the Coherent Optical PArallel Computing project and by the Consortium des Equipements de Calcul Intensif, funded by the FRS-FNRS under Grant 2.5020.11.

1. L. Gyongyosi, S. Imre, A survey on quantum computing technology. *Comput. Sci. Rev.* **31**, 51–71 (2019).
2. National Academies of Sciences, Engineering, and Medicine, *Quantum Computing: Progress and Prospects*, E. Grumbling, M. Horowitz, Eds. (The National Academies Press, Washington, DC, 2019), p. 272.
3. S. Lloyd, M. Mohseni, P. Rebentrost, Quantum principal component analysis. *Nat. Phys.* **10**, 631–633 (2014).
4. P. Rebentrost, B. Gupt, T. R. Bromley, Quantum computational finance: Monte Carlo pricing of financial derivatives. *Phys. Rev. A (Coll. Park)* **98**, 022321 (2018).
5. R. Xia, S. Kais, Quantum machine learning for electronic structure calculations. *Nat. Commun.* **9**, 4195 (2018).
6. M. Schuld, I. Sinayskiy, F. Petruccione, Prediction by linear regression on a quantum computer. *Phys. Rev. A (Coll. Park)* **94**, 022342 (2016).
7. S. Kais, Ed., *Quantum Information and Computation for Chemistry*, (Wiley and Sons, Hoboken, NJ, 2014), Vol. vol. 154.
8. J. Yuen-Zhou, J. J. Krich, I. Kassal, A. S. Johnson, A. Aspuru-Guzik, *Ultrafast spectroscopy: Quantum Information and Wavepackets*, (IOP Publishing, Bristol, 2014).
9. S. Mukamel, *Principles of Nonlinear Optical Spectroscopy*, (Oxford Series in Optical and Imaging Sciences, Oxford University Press, 1995).
10. M. Cho, *Two-Dimensional Optical Spectroscopy*, (CRC Press, Boca Raton, 2009).
11. P. Hamm, M. T. Zanni, *Concepts and Methods of 2D Infrared Spectroscopy*, (Cambridge University Press, Cambridge, 2011).
12. B. Fresch *et al.*, Parallel and multivalued logic by the two-dimensional photon-echo response of a rhodamine–DNA complex. *J. Phys. Chem. Lett.* **6**, 1714–1718 (2015).
13. B. Fresch, D. Hiluf, E. Collini, R. D. Levine, F. Remacle, Molecular decision trees realized by ultrafast electronic spectroscopy. *Proc. Natl. Acad. Sci. U.S.A.* **110**, 17183–17188 (2013).
14. T.-M. Yan, B. Fresch, R. D. Levine, F. Remacle, Information processing in parallel through directionally resolved molecular polarization components in coherent multidimensional spectroscopy. *J. Chem. Phys.* **143**, 064106 (2015).
15. D. B. Turner, Y. Hassan, G. D. Scholes, Exciton superposition states in CdSe nanocrystals measured using broadband two-dimensional electronic spectroscopy. *Nano Lett.* **12**, 880–886 (2012).
16. S. Dong *et al.*, Observation of an excitonic quantum coherence in CdSe nanocrystals. *Nano Lett.* **15**, 6875–6882 (2015).
17. E. Cassette, R. D. Pensack, B. Mahler, G. D. Scholes, Room-temperature exciton coherence and dephasing in two-dimensional nanostructures. *Nat. Commun.* **6**, 6086 (2015).
18. E. M. Janke *et al.*, Origin of broad emission spectra in InP quantum dots: Contributions from structural and electronic disorder. *J. Am. Chem. Soc.* **140**, 15791–15803 (2018).
19. J. R. Caram *et al.*, Exploring size and state dynamics in CdSe quantum dots using two-dimensional electronic spectroscopy. *J. Chem. Phys.* **140**, 084701 (2014).
20. J. R. Caram *et al.*, Persistent inter-excitonic quantum coherence in CdSe quantum dots. *J. Phys. Chem. Lett.* **5**, 196–204 (2014).
21. G. B. Griffin *et al.*, Two-dimensional electronic spectroscopy of CdSe nanoparticles at very low pulse power. *J. Chem. Phys.* **138**, 014705 (2013).
22. C. Y. Wong, G. D. Scholes, Biexcitonic fine structure of CdSe nanocrystals probed by polarization-dependent two-dimensional photon echo spectroscopy. *J. Phys. Chem. A* **115**, 3797–3806 (2011).
23. N. Lenngren *et al.*, Hot electron and hole dynamics in thiol-capped CdSe quantum dots revealed by 2D electronic spectroscopy. *Phys. Chem. Chem. Phys.* **18**, 26199–26204 (2016).
24. E. Collini *et al.*, Quantum phenomena in nanomaterials: Coherent superpositions of fine structure states in CdSe nanocrystals at room temperature. *J. Phys. Chem. C* **123**, 31286–31293 (2019).
25. V. I. Klimov, Ed., *Nanocrystal Quantum Dots*, (CRC Press, Boca Raton, ed. 2, 2010).
26. F. Remacle, R. D. Levine, Architecture with designer atoms: Simple theoretical considerations. *Proc. Natl. Acad. Sci. U.S.A.* **97**, 553–558 (2000).
27. E. Collini, Spectroscopic signatures of quantum-coherent energy transfer. *Chem. Soc. Rev.* **42**, 4932–4947 (2013).
28. F. D. Fuller, J. P. Ogilvie, Experimental implementations of two-dimensional fourier transform electronic spectroscopy. *Annu. Rev. Phys. Chem.* **66**, 667–690 (2015).
29. J. C. Dean, G. D. Scholes, Coherence spectroscopy in the condensed phase: Insights into molecular structure, environment, and interactions. *Acc. Chem. Res.* **50**, 2746–2755 (2017).
30. T. A. A. Oliver, Recent advances in multidimensional ultrafast spectroscopy. *R. Soc. Open Sci.* **5**, 171425 (2018).
31. J. R. Caram, G. S. Engel, Extracting dynamics of excitonic coherences in congested spectra of photosynthetic light harvesting antenna complexes. *Faraday Discuss.* **153**, 93–104 (2011).

32. G. Panitchayangkoon *et al*., Direct evidence of quantum transport in photosynthetic light-harvesting complexes. *Proc. Natl. Acad. Sci. U.S.A.* **108**, 20908–20912 (2011).
33. Z. Hu, G. S. Engel, S. Kais, Double-excitation manifold's effect on exciton transfer dynamics and the efficiency of coherent light harvesting. *Phys. Chem. Chem. Phys.* **20**, 30032–30040 (2018).
34. S.-H. Yeh, R. D. Hoehn, M. A. Allodi, G. S. Engel, S. Kais, Elucidation of near-resonance vibronic coherence lifetimes by nonadiabatic electronic-vibrational state character mixing. *Proc. Natl. Acad. Sci. U.S.A.* **116**, 18263–18268 (2019).
35. Y. Alhassid, The statistical theory of quantum dots. *Rev. Mod. Phys.* **72**, 895–968 (2000).
36. T. A. Brody *et al*., Random-matrix physics: Spectrum and strength fluctuations. *Rev. Mod. Phys.* **53**, 385–479 (1981).
37. E. Cohen *et al*., Fast energy transfer in CdSe quantum dot layered structures: Controlling coupling with covalent-bond organic linkers. *J. Phys. Chem. C* **122**, 5753–5758 (2018).
38. L. Brus, Electronic wave functions in semiconductor clusters: Experiment and theory. *J. Phys. Chem.* **90**, 2555–2560 (1986).
39. K. Leung, S. Pokrant, K. B. Whaley, Exciton fine structure in CdSe nanoclusters. *Phys. Rev. B Condens. Matter Mater. Phys.* **57**, 12291–12301 (1998).
40. A. L. Efros, M. Rosen, The electronic structure of semi-conducting nanocrystal. *Ann. Rev. Mater. Sci.* **30**, 475–521 (2000).
41. A. L. Efros *et al*., Band-edge exciton in quantum dots of semiconductors with a degenerate valence band: Dark and bright exciton states. *Phys. Rev. B Condens. Matter* **54**, 4843–4856 (1996).
42. S. Lee, L. Jönsson, J. W. Wilkins, G. W. Bryant, G. Klimeck, Electron-hole correlations in semiconductor quantum dots with tight-binding wave functions. *Phys. Rev. B Condens. Matter Mater. Phys.* **63**, 195318 (2001).
43. L. W. Wang, A. Zunger, High-energy excitonic transitions in CdSe quantum dots. *J. Phys. Chem. B* **102**, 6449–6454 (1998).
44. O. V. Prezhdo, Photoinduced dynamics in semiconductor quantum dots: Insights from time-domain ab initio studies. *Acc. Chem. Res.* **42**, 2005–2016 (2009).
45. J. M. Luttinger, W. Kohn, Motion of electrons and holes in perturbed periodic fields. *Phys. Rev.* **97**, 869–883 (1955).
46. A. L. Efros, Luminescence polarization of CdSe microcrystals. *Phys. Rev. B Condens. Matter* **46**, 7448–7458 (1992).
47. H. Gattuso, B. Fresch, D. R. Levine, F. Remacle, Coherent exciton dynamics in ensembles of size-dispersed CdSe quantum dot dimers probed via ultrafast spectroscopy: A quantum computational study. *Appl. Sci.* **10**, 1328 (2020).
48. J. Hinze, Ed., *The Unitary Group for the Evaluation of the Electronic Energy Matrix Elements*, (Springer-Verlag, Berlin, 1981), Vol. 22.
49. R. Gilmore, *Lie Groups, Lie Algebras and Some of Their Applications*, (Mineola, Dover, 2012).
50. Y. Alhassid, R. D. Levine, Connection between the maximal entropy and the scattering theoretic analyses of collision processes. *Phys. Rev. A* **18**, 89–116 (1978).
51. A. J. F. Siegert, On the approach to statistical equilibrium. *Phys. Rev.* **76**, 1708–1714 (1949).
52. R. I. Cukier, K. E. Shuler, On the microscopic conditions for linear macroscopic laws. *J. Chem. Phys.* **57**, 302–311 (1972).
53. Wikipedia, Cumulants (2020). https://en.wikipedia.org/wiki/Cumulant. Accessed 7 April 2020.
54. M. Abramovitz, I. Stegun, *A Handbook of Mathematical Functions*, (Dover, New York, 1972).